

Comparison of 3.6 – 8.0 Micron *Spitzer*/IRAC Galactic Center Survey Point Sources with Chandra X–Ray Point Sources in the Central 40x40 Parsecs

R. G. Arendt^{1,2}, D. Y. Gezari³, S. R. Stolovy⁴, K. Sellgren⁵, R. Smith⁶, S. V. Ramírez⁷,
F. Yusef-Zadeh⁸, C. J. Law^{8,9}, H. A. Smith¹⁰, A. S. Cotera¹¹, S. H. Moseley¹²

ABSTRACT

We have studied the correlation between 2357 Chandra X–ray point sources in a 40×40 parsec field and $\sim 20,000$ infrared sources we observed in the corresponding subset of our $2^\circ \times 1.4^\circ$ *Spitzer*/IRAC Galactic Center Survey at 3.6–8.0 μm , using various spatial and X–ray hardness thresholds. The correlation was determined for source separations of less than $0''.5$, $1''$ or $2''$. Only the soft X–ray sources show any correlation with infrared point sources on these scales, and that correlation is very weak. The upper limit on hard X–ray sources that have infrared counterparts is $< 1.7\%$ (3σ). However, because of the confusion limit of the IR catalog, we only detect IR sources with absolute magnitudes $\lesssim 1$. As a result, a stronger correlation with fainter sources cannot be ruled out. Only

¹CRESST/UMBC/GSFC, Code 665, NASA/Goddard Space Flight Center, 8800 Greenbelt Road, Greenbelt, MD 20771; richard.g.arendt@nasa.gov

²Science Systems and Applications, Inc.

³NASA/Goddard Space Flight Center, Code 667, 8800 Greenbelt Road, Greenbelt, MD 20771

⁴*Spitzer* Science Center, California Institute of Technology, Mail Code 220-6, 1200 East California Boulevard, Pasadena, CA 91125

⁵Department of Astronomy, Ohio State University, 140 West 18th Av., Columbus, OH, 43210, USA

⁶NASA/Goddard Space Flight Center, Code 662, 8800 Greenbelt Road, Greenbelt, MD 20771

⁷IPAC, California Institute of Technology, Mail Code 100-22, 1200 East California Boulevard, Pasadena, CA 91125

⁸Department of Physics and Astronomy, Northwestern University, Evanston, IL 60208

⁹now at Sterrenkundig Instituut “Anton Pannekoek”, Universiteit van Amsterdam

¹⁰Harvard-Smithsonian Center for Astrophysics, 60 Garden Street, Cambridge, MA 02138

¹¹SETI Institute, 515 North Whisman Road, Mountain View, CA 94043

¹²NASA/Goddard Space Flight Center, Code 665, 8800 Greenbelt Road, Greenbelt, MD 20771

one compact infrared source, IRS 13, coincides with any of the dozen prominent X-ray emission features in the 3×3 parsec region centered on Sgr A*, and the diffuse X-ray and infrared emission around Sgr A* seems to be anti-correlated on a few-arcsecond scale. We compare our results with previous identifications of near-infrared companions to Chandra X-ray sources.

Subject headings: Galaxy: center — infrared: stars — X-rays: binaries

1. Introduction

X-ray surveys of the Galactic center with *Chandra X-Ray Observatory* (Wang et al. 2002; Munro et al. 2003) have provided a deep sampling of the population of X-ray point sources that shows a large increase in source density toward the Galactic Center. These X-ray sources have been modeled as a population mix of various sorts of X-ray binaries, Wolf-Rayet stars, nearby X-ray active stars in the foreground, and background AGN (Pfahl et al. 2002; Belczynski & Taam 2004; Ebisawa et al. 2005; Ruiter et al. 2006; Liu & Li 2006; Munro et al. 2006). However, the high extinction toward the Galactic center prohibits the detection of visible light emitted by the stellar components in the expected binaries. Near-IR searches have also had little success in detecting IR counterparts of the X-ray point sources. Several OB stars and Wolf-Rayet stars have been identified with X-ray sources by near-IR spectroscopy (Munro et al. 2006, Mikles et al. 2006, Mauerhan et al. 2007), but the paucity of near-IR detections sets limits that suggest only a small fraction of the X-ray sources can be high mass X-ray binaries (HMXBs; Laycock et al. 2005; Bandopadhyay et al. 2006).

Our *Spitzer Space Telescope* IRAC survey of the Galactic Center (Stolovy et al. 2006, S. Stolovy et al. 2008 in preparation) provides a new opportunity to search for IR counterparts to the X-ray sources. IRAC observations cover four broad bands at 3.6, 4.5, 5.8 and 8 μm . The survey imaged a $2.0^\circ \times 1.4^\circ$ (280×200 parsec at 8.0 kpc) region of the Galactic Center with a nominal resolution of $\sim 2''$ (Figure 1). Since our observations are at longer wavelengths than ground-based near-IR (*J, H, K*) observations, extinction should be less of a hindrance to the detection of stellar companions. Furthermore, at the longest IRAC wavelengths (5.8 and especially 8 μm), IRAC is sensitive to circumstellar dust emission which may cause significant extinction at shorter wavelengths. Thus, comparison of the X-ray and IR point source catalogs may reveal stellar companions which are at an evolutionary stage where they produce large quantities of dust, or are simply too heavily attenuated by the line of sight extinction at shorter wavelengths.

We calculated the correlation between 2357 hard and soft Chandra X-ray sources iden-

tified and catalogued by Muno et al. (2003) and the $\sim 20,000$ *Spitzer*/IRAC infrared point sources that lie within a 40×40 parsec (20×20 arcmin) field at the Galactic Center (Figure 2). The IR sources are a small subset of our full catalog (Ramírez et al. 2008) which has a mean confusion limit of $[3.6] = 12.4$ mag. We divide the Chandra sources by their hardness because the high column density of gas towards the GC, $N_H \sim 5 \times 10^{22}$ cm $^{-2}$, absorbs all soft X-rays. Thus soft X-ray sources must be in the foreground towards the GC; hard X-ray sources can be at the 8 kpc distance of the GC or can be foreground/background sources.

2. Analysis

2.1. IR/X-ray Point Source Correlations

The positional uncertainty of the IRAC point sources is correlated with wavelength. In the final band-merged catalog, the reported position is that measured at the shortest IRAC wavelength at which each source was detected. Within a radius of $10'$ from the galactic center 86% of the IRAC sources are detected at 3.6 or 4.5 μm . According to Ramírez et al. (2008), 90% of these sources have positional errors of $< 0.16''$. The positional uncertainties of the X-ray sources are reported by Muno et al. (2003) to be increasing with distance from the center of the field. Based on the given information, we have assigned uncertainties to the X-ray positions that are the larger of $0'.3$ or $0.209'' e^{\theta/225''}$, where θ is the distance from the center of the field. With this prescription, only 39 of the 2357 X-ray sources have positional uncertainties $> 2'.5$, and 1645 ($\sim 70\%$) have uncertainties $< 0'.8$.

In light of these positional uncertainties, we searched for infrared sources that fell within three different limits ($0'.5$, $1''$ and $2''$) of the Muno et al. (2003) X-ray source positions. The tightest constraint here ($0'.5$), should include all associations between infrared and X-ray sources with high positional accuracies. Some associations between sources with larger positional errors may be missed, but the tight limit will best exclude coincidental associations between unrelated sources along the same line of sight. The looser limits were employed to provide a more complete census of the total number of possible associations, and to provide a statistical test for random unrelated associations, which should increase directly proportionally to the area of the constraint.

Figures 3a and 4a show all the X-ray source locations plotted on the IRAC 3.6 and 8 μm images. Figures 3b and 4b show only the X-ray sources with IR counterparts within the specified limits ($< 2''$, $1''$, $0'.5$ are red, green and blue symbols respectively). Figure 5a–b illustrates the cataloged distribution of IR sources and X-ray sources. The distribution of IR sources appears uniform only because it is confusion limited. For stars much brighter

than the confusion limit, the density is peaked at the Galactic center (Ramírez et al. 2008) as is that of the X-ray sources.

The number of X-ray sources N found coincident with an IR source, for each of the three radial constraints and at each IRAC wavelength is listed in Table 1. The statistical uncertainty on N is given by $\sigma_N = \sqrt{N}$. The X-ray and infrared sources in the study field show an extremely weak correlation. Fewer than 7% of the 2357 X-ray sources had 3.6 μm counterparts in the catalog of IRAC infrared sources in a 1'' sampling radius, and most of these are likely to be false identifications. The number of counterparts decreases with increasing wavelength.

2.2. Likelihood of Chance Associations

We determined the likelihood of false correlations in the crowded infrared field by repeating the same correlation analysis eight additional times, but with the X-ray source position template offset from the nominal location, in a 5''-pitch regular grid of eight positions N-S and E-W of center. Figure 5c shows the distribution of the X-ray sources with 3.6 μm counterparts (within 1''), and Figure 5d shows the distribution when the IR sources are artificially offset by 5''. The mean number of X-ray sources with IR counterparts in these offset comparisons is listed in Table 1 as M , with $\sigma_M = \sqrt{M/8}$. The number of coincidences found in excess of chance is $N - M$. This excess is typically 1% of the X-ray sources, and never larger than 3 times the statistical uncertainty. However, the fact that M increases proportionally to the area of the matching constraint, while N increases more slowly, is another indication that (depending on wavelength) roughly 10-30 of the matching IR and X-ray sources are real associations. There are no cases of multiple candidates within circles of 0.5'' or 1'', and only 11 sources with 2 candidates within a 2'' circle. These numbers are lower than expected by random chance because the width of the IRAC beam prevents resolving sources that are closer together than $\sim 3''$.

As some of the X-ray sources do have fairly large positional uncertainties, we have repeated the matching using only the X-ray sources with uncertainties $< 0.8''$. These results are shown in Table 2. Qualitatively, the results are similar to Table 1, in that the offset matching tests usually find fewer matches than the properly aligned tests. Also the number of matching sources (N) again rises more slowly than is expected (and measured by M) for purely random associations. However, because the overall sample size is reduced by a factor of 0.7, the results are not as statistically significant as those obtained using the full sample.

An interesting difference appears if we separate the X-ray sources according to their

spectral hardness. There is a modest excess in the number of soft X-ray sources (defined as those with detections in the 0.5–2.0 keV band) with infrared counterparts above that expected from random chance (Table 3). There is a 4σ excess in the number of soft X-ray sources with IR counterparts at $3.6 \mu\text{m}$ compared to a 2σ excess in the correlations at $8.0 \mu\text{m}$. Again the trend persists, but with lower statistical significance, if we limit the X-ray data set to those sources with positional uncertainties $< 0''.8$ (Table 4). Based on the soft X-rays observed from these sources (and therefore their relatively low column densities), we expect that the soft X-ray sources are foreground objects, and not at the distance of the Galactic Center. The excess soft X-ray/IR correlation is therefore likely due to these sources being nearby, rather than being intrinsically bright in both wavebands. In contrast, the hard X-ray sources seem to have only as many infrared counterparts as would be expected from random associations (Tables 5 and 6). This is indicated both by the comparison of the aligned and offset matching (N vs. M), and by the way N increases proportionally to the area of the matching constraint.

3. Results

We provide a listing of IR and X-ray sources coincident within $1''$ in Table 7. The table is provided to facilitate follow up research on these sources, but we remind the reader that the majority of these associations are likely to be merely coincidental. The table contains designations and coordinates from each catalog, along with the IR magnitudes, an indication X-ray spectral hardness, and the actual separation between the associated sources. Much additional information can be found by consulting the original catalogs (Muno et al. 2003; Ramírez et al. 2008).

3.1. Nature of the Correlations

The spatial distribution of soft X-ray sources is less concentrated toward the Galactic Center than that of the hard sources. Figure 6 shows the cumulative distributions of distance from Sgr A* for all X-ray sources and for the hard and soft sources separately. Also shown is the distribution of the 51 sources which had $3.6 \mu\text{m}$ IR counterparts within $0''.5$. These distributions can be compared statistically using the Kolmogorov–Smirnov (K–S) test (e.g. Press et al. 1986). This test measures the maximum separation D between two cumulative distributions. Then we calculate that probability of having the two distributions differ by D or larger, under the assumption that they are sampled from the same parent distribution. By this statistic, the probability of finding the observed $D(\text{hard} - \text{soft})$ is essentially 0, if the

two types of X-ray source really have the same radial spatial distribution with respect to Sgr A*. The probability of finding the observed $D(\text{hard} - 3.6\mu\text{m})$ is 0.01, and the probability of finding the observed $D(\text{soft} - 3.6\mu\text{m})$ is 0.72. Thus, the K-S test indicates that it is statistically unlikely that the hard X-ray sources and the set of matching $3.6\mu\text{m}$ IR sources share the same degree of clustering toward the Galactic Center. Whereas the distribution of the matching $3.6\mu\text{m}$ IR associations is entirely consistent with that of the soft X-ray sources. This is further evidence that a substantial majority of IR counterparts are associated with the soft X-ray sources rather than the more numerous hard sources. For comparison the distribution of all $3.6\mu\text{m}$ sources within the same area of the X-ray sources is also shown in Figure 6. As would be inferred from Figure 5a, this distribution is very close to (but not exactly) uniform. The probability of finding $D(\text{uniform} - \text{all } 3.6\mu\text{m})$ is 0.03.

3.2. Infrared Colors of Counterparts to X-ray Sources

We next investigated the colors of the potential IR counterparts, to see if they might be useful for separating intrinsic IR/X-ray sources from the random associations. The color-magnitude diagram for the 17613 IRAC sources in the 40×40 parsec study region that were detected at both 3.6 and $4.5\mu\text{m}$ is shown in Figure 7. The circles and squares indicate IR stars that are identified with hard and soft X-ray sources, respectively, in the Munro et al. (2003) catalog. 42 X-ray sources had IRAC sources falling within $0''.5$ of the nominal X-ray positions (large circles/squares), 130 had IRAC sources within $1''$ (medium circles/squares), and 394 had IRAC sources falling within $2''$ (small circles/squares). See Tables 1–3 for details, including statistics for hard and soft X-ray sources.

The colors of the possible infrared counterparts do not seem to be unusual in any way. The distribution of colors of those infrared stars that have coincident X-ray sources is essentially the same as the distribution of all other infrared stars in our sample. There is also no apparent differentiation between the colors of infrared stars as a function of their distance from the X-ray source. The K-S test reveals no significant difference between the color distributions of the infrared candidates and the larger sample of all infrared sources within the field. Thus, the observed colors of the IRAC point sources are of little use in attempting to discriminate between real and coincidental X-ray/IR correlations.

3.3. Infrared and X-ray Sources at the Central Parsec

Casual inspection of the Chandra and *Spitzer*/IRAC images gives the impression that the bright X-ray cluster at the Galactic Center is well-correlated with the infrared emission. However, closer examination shows that only one of the bright, compact mid-infrared sources, IRS 13, coincides with any of the discrete X-ray sources in the central 3×3 parsecs (Figure 8). The separation between the X-ray and IRAC positions is $< 1''$ (see source SSTGC 0524504 in Table 7). Notably, IRS 13 has been proposed as a candidate host for an intermediate black hole (Maillard et al. 2004). While we do also detect IRS 10* (= IRS 10EE), the mid-infrared counterpart to an SiO maser source, with *Spitzer*/IRAC, and Peeples et al. (2007) identify a Chandra X-ray source with IRS 10*, that X-ray source is more than $2''$ east of IRS 10* so it does not meet our correlation criteria. Peeples et al. (2007) find spatial coincidences between Chandra X-ray sources and five other point sources they observe at 1.6 and $2.2 \mu\text{m}$, but we do not detect any of these sources with *Spitzer*/IRAC. Thus, with the exception of IRS 13, none of the point sources in the central 3×3 parsecs imaged in the *Spitzer*/IRAC $3.6 - 8.0 \mu\text{m}$ survey, and none of the compact $12 \mu\text{m}$ IRS sources imaged with sub-arcsec resolution by Gezari et al. (1996), have X-ray counterparts. The X-ray emission in the immediate vicinity of Sgr A* is discussed in Gezari et al. (2006).

4. Discussion

Several population studies have been done to estimate what the relative contributions of different X-ray sources are to the Galactic Center catalog of Munro et al. (2003) or other Galactic Center X-ray surveys. These models give insight into what infrared counterparts we might hope to find with *Spitzer*/IRAC. The Galactic Center is thought to contain a mix of CVs, magnetically accreting CVs (intermediate polars), low-mass X-ray binaries (LMXBs), high-mass X-ray binaries (HMXBs), massive stars with strong winds, colliding wind binaries, and pulsars (Pfahl et al. 2002; Belczynski & Taam 2004; Ruiter et al. 2006; Liu & Li 2006; Munro et al. 2006). We would like to know which of these are most likely to be detectable at a distance of 8 kpc with *Spitzer*/IRAC. The donor stars for HMXBs, massive stars with strong winds, and colliding wind binaries are O stars and Wolf-Rayet stars. These stars are luminous enough to be detected with *Spitzer*/IRAC, especially if they have circumstellar dust or heat the surrounding interstellar medium. The donor stars for CVs, intermediate polars, and LMXBs are probably not luminous enough to be detected with *Spitzer*/IRAC unless they are a red giant or they are surrounded by circumstellar dust.

The INTEGRAL gamma-ray observatory has discovered a new class of hard X-ray source in the Galactic plane: highly obscured HMXBs, with hydrogen column densities

much higher than predicted by their extinction, due to intrinsic absorption in the wind of the supergiant secondary (Dean et al. 2005; Walter et al. 2006). *Spitzer*/IRAC photometry of highly obscured supergiant HMXBs has detected moderate infrared excesses from a hot dust component, but with roughly a 25% success rate (Kaplan et al. 2006; Rahoui et al. 2008). However, none of these cases show evidence for a large mass of cooler dust in the systems, which could lead to a rising mid-IR spectrum at wavelengths $\gtrsim 5\mu\text{m}$. Our lack of detection of a large number of $8\mu\text{m}$ counterparts suggests that the GC X-ray sources also lack massive dusty shells.

Pfahl et al. (2002) conclude that most of the X-ray sources found by Wang et al. (2002), in a wider but shallower Chandra survey of the Galactic Center, are HMXBs: neutron stars with O or B star companions. Other authors, however, conclude that only a small fraction of the Muno et al. (2003) Galactic Center X-ray sources are associated with massive stars (Belczynski & Taam 2004; Ruitter et al. 2006; Liu & Li 2006; Muno et al. 2006). Muno et al. (2006), Mikles et al. (2006), and Mauerhan et al. (2007) have combined Chandra point source catalogs of the Galactic Center with the 2MASS catalog to find candidate massive stars. Muno et al. (2006) also includes 3.6 cm radio data. They discard all soft X-ray sources, because the interstellar absorption to the Galactic Center will absorb all soft X-ray emission from there. They also discard all 2MASS sources with blue J-K colors as being foreground sources, because the interstellar extinction to the Galactic Center reddens all sources there. They use near-IR spectra to identify three (Muno et al. 2006), one (Mikles et al. 2006), and two (Mauerhan et al. 2007) massive stars in the Galactic Center with X-ray emission. That so much effort has gone into identifying a total of six massive stars with X-ray emission, either from colliding winds or from accretion onto a compact companion, out of more than a thousand hard X-ray sources in the Galactic Center, underscores the difficulty of observing infrared emission from the donor stars for X-ray sources in the Galactic Center.

Bandyopadhyay et al. (2005), reported that roughly 75% of a sample of 77 hard X-ray sources had faint ($K = 13-20$) candidate K-band counterparts within a $1''.3$ radius. However, they noted that this is exactly the number of random associations that they predict from a Monte Carlo simulation. Thus although Bandyopadhyay et al. (2005) identified 58 K-band “candidates” none of these sources are likely to be real infrared counterparts to the hard X-ray sources in their sample. Correlations at H and J bands did show small statistical excess above the randomly expected number of associations. Follow-up spectroscopic observations by Bandyopadhyay et al. (2006) failed to find indications of accretion (e.g. Br γ emission) among 28 candidates observed. They conclude that the apparent associations are merely foreground stars, and that the X-ray sources are likely dominated by a population of low mass X-ray binaries (LMXBs) and cataclysmic variables (CVs) with $K > 20$. Laycock et al. (2005) compared 1453 hard and 105 soft X-ray sources with near infrared stars from

the 2MASS survey and concluded that high-mass X-ray binaries are not the dominant hard X-ray source population.

Unlike the hard X-ray sources examined by Bandyopadhyay et al. (2006), we clearly do detect (if only in a statistical sense) a population of sources with both soft X-ray and infrared emission, notably in the 3.6 and 4.5 μm bands (a net excess of $\sim 34 \pm 8$ sources in these bands when a positional agreement of $< 1''$ is required; see Table 3). These sources represent $\sim 6\%$ of the complete soft X-ray sample and, as noted previously, are likely foreground sources rather than being intrinsically bright in IR and X-rays. Ebisawa et al. (2005) observed a blank part of the galactic plane with Chandra, and were able to find 2MASS identifications for almost all their soft X-ray sources; they concluded they were nearby active stars on the main sequence. For comparison, Sidoli et al. (2001) found 107 sources in a 12 deg² region around the GC surveyed with the ROSAT PSPC, which was sensitive to X-rays between 0.1–2.4 keV. Of these 107, they identified 20 (or 19%) as being associated with stars, noting that these have softer or less absorbed spectra. Although our data cannot conclusively determine if the softer X-ray sources with IR counterparts are indeed from a different population than the sources without counterparts, this could be tested with more observations and may represent a method to eliminate foreground sources from a GC catalog.

The donor stars in both LMXBs and CVs at the GC are expected to be too faint to be detected in our IRAC survey. Over the full IRAC GC survey, Ramírez et al. (2008) set mean confusion limits at 12.4, 12.1, 11.7 and 11.2 mag for 3.6, 4.5, 5.8 and 8 μm respectively. However, because of the general increase in the volume density of stars with decreasing distance from the Galactic Center, confusion limits are about 2 magnitudes brighter in the vicinity of Sgr A (see Fig. 8 of Ramírez et al. 2008). Given a distance modulus of 7.26 and extinction of about 1.5 - 2 magnitudes, scaled from $A_K \approx 3.3$ (Blum et al. 1996), using either the Indebetouw et al. (2005) or Flaherty et al. (2007) extinction laws, we should only detect sources with absolute magnitudes $\lesssim 1$. Variations in extinction across the region may alter the apparent magnitudes of some IR sources, but the main limitation of the IRAC survey is due to confusion, not extinction nor sensitivity. At 8 μm and to a lesser degree at 5.8 μm , a large instrumental beam, and confusion from the diffuse ISM are additional limitations which reduce the number of sources detected compared to 3.6 and 4.5 μm . While the extinction is not the dominant factor in the detection of the IR sources, it is interesting to note that extinction appears to have a strong effect on the distribution of the X-ray sources. In Figures 3a and 4a, there is an evident correlation between a relatively low X-ray source density and an IR dark cloud (IRDC) to the southeast of the Galactic Center.

5. Conclusions

We have analyzed the possible correlations between the largest number of candidate sources to date: 2357 X-ray sources (of which 1809 are hard X-ray sources most likely located at the Galactic Center) and $\sim 20,000$ *Spitzer*/IRAC infrared point sources. Source confusion limits our correlations to only bright infrared sources with absolute magnitudes $\lesssim 1$ if located near the Galactic Center. The lack of any significant correlation between hard X-ray sources and $3.6 - 8 \mu\text{m}$ infrared point sources suggests that there is no unique population of sources that are bright at both X-ray and $3.6 - 8 \mu\text{m}$ wavelengths. Based on this study, we can set the upper limit on the fraction of all hard X-ray sources that can be bright at both X-ray and $3.6 - 8 \mu\text{m}$ wavelengths to be $< 1.7\%$ (3σ).

This work is based on observations made with the Spitzer Space Telescope, which is operated by the Jet Propulsion Laboratory, California Institute of Technology under a contract with NASA. Support for this work was provided by NASA. KS thanks the NASA Faculty Fellowship Program for financial support and the hospitality of JPL's Long Wavelength Center and the Spitzer Science Center. We thank the referee for substantial comments and suggestions.

REFERENCES

- Bandyopadhyay, R. M., et al. 2005, MNRAS, 364, 1195
- Bandyopadhyay, R. M., Gosling, A. J., Blundell, K. M., Podsiadlowski, P., Einkenberry, S. A., Mikles, V. J., Miller-Jones, J. C. A., & Bauer, F. E. 2006, VI Microquasar Workshop: Microquasars and Beyond
- Belczynski, K., & Taam, R. E. 2004, ApJ, 616, 1159
- Blum, R. D., Sellgren, K., & Depoy, D. L. 1996, ApJ, 470, 864
- Dean, A. J., et al. 2005, A&A, 443, 485
- Ebisawa, K., et al. 2005, ApJ, 635, 214
- Flaherty, K. M., Pipher, J. L., Megeath, S. T., Winston, E. M., Gutermuth, R. A., Muzerolle, J., Allen, L. E., & Fazio, G. G. 2007, ApJ, 663, 1069
- Gezari, D., Dwek, E., & Varosi, F., 1996, Proc. Symposium 169 of the IAU, ed. L. Blitz & P. Teuben, 231

- Gezari, D. Y., et al. 2006, *Journal of Physics Conference Series*, 54, 171
- Ghez, A., et al. 2005, *ApJ*, 635, 1087
- Indebetouw, R., et al. 2005, *ApJ*, 619, 931
- Kaplan, D. L., Moon, D.-S., & Reach, W. T. 2006, *ApJ*, 649, L107
- Laycock, S., Grindlay, J., van den Berg, M., Zhao, P., Hong, J., Koenig, X., Schlegel, E. M., & Persson, S. E. 2005, *ApJ*, 634, L53
- Liu, X.-W., & Li, X.-D. 2006, *A&A*, 449, 135
- Maillard, J. P., Paumard, T., Stolovy, S. R., Rigaut, F. 2004, *A&A*, 423, 155
- Mauerhan, J. C., Munro, M. P., & Morris, M. 2007, *ApJ*, 662, 574
- Mikles, V. J., Eikenberry, S. S., Munro, M. P., Bandyopadhyay, R. M., & Patel, S. 2006, *ApJ*, 650, 203
- Munro, M. P., et al. 2003, *ApJ*, 589, 225
- Munro, M. P., Bower, G. C., Burgasser, A. J., Baganoff, F. K., Morris, M. R., & Brandt, W. N. 2006, *ApJ*, 638, 183
- Peeples, M. S., Stanek, K. Z., & Depoy, D. L. 2007, *AcA*, 57, 173
- Pfahl, E., Rappaport, S., & Podsiadlowski, P. 2002, *ApJ*, 571, L37
- Press, W. H., Flannery, B. P., Teukolsky, S. A., & Vetterling, W. T. 1986, *Numerical Recipes: The Art of Scientific Computing*, (Cambridge: Cambridge University Press)
- Rahoui, F., Chaty, S., Lagage, P.-O., & Pantin, E. 2008, arXiv:0802.2410
- Ramírez, S. V., et al. 2008, *ApJS*, 175, 147
- Ruiter, A. J., Belczynski, K., & Harrison, T. E. 2006, *ApJ*, 640, L167
- Sidoli, L., Belloni, T., & Mereghetti, S. 2001, *A&A*, 368, 835
- Stolovy S., et al. 2006, *J. Phys. Conf. Series*, 54, 176
- Walter, R., et al. 2006, *A&A*, 453, 133
- Wang, Q. D., Gotthelf, E. V., & Lang, C. C. 2002, *Nature*, 415, 148

Table 1. All X-ray Sources (2357)

Wavelength (μm)	N	σ_N	M	σ_M	$N - M$	σ_{N-M}	$(N - M)/\sigma_{N-M}$
Positional agreement $< 0.5''$							
3.6	51	7.1	30.5	2.0	20.5	7.4	2.8
4.5	46	6.8	27.8	1.9	18.2	7.0	2.6
5.8	35	5.9	19.9	1.6	15.1	6.1	2.5
8	22	4.7	10.1	1.1	11.9	4.8	2.5
Positional agreement $< 1.0''$							
3.6	156	12.5	120.4	3.9	35.6	13.1	2.7
4.5	137	11.7	108.2	3.7	28.8	12.3	2.3
5.8	104	10.2	77.4	3.1	26.6	10.7	2.5
8	64	8.0	42.0	2.3	22.0	8.3	2.6
Positional agreement $< 2.0''$							
3.6	488	22.1	458.4	7.6	29.6	23.4	1.3
4.5	424	20.6	414.5	7.2	9.5	21.8	0.4
5.8	320	17.9	297.9	6.1	22.1	18.9	1.2
8	179	13.4	170.9	4.6	8.1	14.2	0.6

Table 2. All X-ray Sources with Uncertainty $< 0''.8$ (1645)

Wavelength (μm)	N	σ_N	M	σ_M	$N - M$	σ_{N-M}	$(N - M)/\sigma_{N-M}$
Positional agreement $< 0.5''$							
3.6	29	5.4	20.5	1.6	8.5	5.6	1.5
4.5	27	5.2	18.2	1.5	8.8	5.4	1.6
5.8	19	4.4	13.0	1.3	6.0	4.5	1.3
8.0	11	3.3	6.2	0.9	4.8	3.4	1.4
Positional agreement $< 1.0''$							
3.6	97	9.8	86.0	3.3	11.0	10.4	1.1
4.5	86	9.3	75.8	3.1	10.2	9.8	1.0
5.8	66	8.1	55.5	2.6	10.5	8.5	1.2
8.0	37	6.1	29.4	1.9	7.6	6.4	1.2
Positional agreement $< 2.0''$							
3.6	328	18.1	324.9	6.4	3.1	19.2	0.2
4.5	272	16.5	290.9	6.0	-18.9	17.6	-1.1
5.8	213	14.6	210.4	5.1	2.6	15.5	0.2
8.0	121	11.0	118.6	3.9	2.4	11.7	0.2

Table 3. Soft X-ray Sources (548)

Wavelength (μm)	N	σ_N	M	σ_M	$N - M$	σ_{N-M}	$(N - M)/\sigma_{N-M}$
Positional agreement $< 0.5''$							
3.6	28	5.3	5.8	0.8	22.2	5.4	4.2
4.8	23	4.8	5.1	0.8	17.9	4.9	3.7
5.8	17	4.1	3.5	0.7	13.5	4.2	3.2
8	8	2.8	1.5	0.4	6.5	2.9	2.3
Positional agreement $< 1.0''$							
3.6	64	8.0	26.4	1.8	37.6	8.2	4.6
4.5	55	7.4	24.1	1.7	30.9	7.6	4.1
5.8	37	6.1	15.9	1.4	21.1	6.2	3.4
8	20	4.5	7.2	1.0	12.8	4.6	2.8
Positional agreement $< 2.0''$							
3.6	126	11.2	103.0	3.6	23.0	11.8	2.0
4.5	109	10.4	95.1	3.4	13.9	11.0	1.3
5.8	78	8.8	69.2	2.9	8.8	9.3	0.9
8	42	6.5	37.4	2.2	4.6	6.8	0.7

Table 4. Soft X-ray Sources with Uncertainty $< 0''.8$ (303)

Wavelength (μm)	N	σ_N	M	σ_M	$N - M$	σ_{N-M}	$(N - M)/\sigma_{N-M}$
Positional agreement $< 0.5''$							
3.6	16	4.0	3.2	0.6	12.8	4.1	3.1
4.5	14	3.7	2.9	0.6	11.1	3.8	2.9
5.8	9	3.0	1.6	0.5	7.4	3.0	2.4
8.0	3	1.7	0.9	0.3	2.1	1.8	1.2
Positional agreement $< 1.0''$							
3.6	34	5.8	15.4	1.4	18.6	6.0	3.1
4.5	30	5.5	13.9	1.3	16.1	5.6	2.9
5.8	19	4.4	8.6	1.0	10.4	4.5	2.3
8.0	9	3.0	4.2	0.7	4.8	3.1	1.5
Positional agreement $< 2.0''$							
3.6	68	8.2	58.4	2.7	9.6	8.7	1.1
4.5	57	7.5	54.0	2.6	3.0	8.0	0.4
5.8	40	6.3	37.4	2.2	2.6	6.7	0.4
8.0	21	4.6	21.0	1.6	0.0	4.9	0.0

Table 5. Hard X-ray Sources (1809)

Wavelength (μm)	N	σ_N	M	σ_M	$N - M$	σ_{N-M}	$(N - M)/\sigma_{N-M}$
Positional agreement $< 0.5''$							
3.6	23	4.8	24.8	1.8	-1.8	5.1	-0.3
4.5	23	4.8	22.6	1.7	0.4	5.1	0.1
5.8	18	4.2	16.4	1.4	1.6	4.5	0.4
8	14	3.7	8.6	1.0	5.4	3.9	1.4
Positional agreement $< 1.0''$							
3.6	92	9.6	94.0	3.4	-2.0	10.2	-0.2
4.5	82	9.1	84.1	3.2	-2.1	9.6	-0.2
5.8	67	8.2	61.5	2.8	5.5	8.6	0.6
8	44	6.6	34.8	2.1	9.2	7.0	1.3
Positional agreement $< 2.0''$							
3.6	362	19.0	355.4	6.7	6.6	20.2	0.3
4.5	315	17.7	319.4	6.3	-4.4	18.8	-0.2
5.8	242	15.6	228.6	5.3	13.4	16.4	0.8
8	137	11.7	133.5	4.1	3.5	12.4	0.3

Table 6. Hard X-ray Sources with Uncertainty $< 0.8''$ (1342)

Wavelength (μm)	N	σ_N	M	σ_M	$N - M$	σ_{N-M}	$(N - M)/\sigma_{N-M}$
Positional agreement $< 0.5''$							
3.6	13	3.6	17.2	1.5	-4.2	3.9	-1.1
4.5	13	3.6	15.4	1.4	-2.4	3.9	-0.6
5.8	10	3.2	11.4	1.2	-1.4	3.4	-0.4
8.0	8	2.8	5.4	0.8	2.6	2.9	0.9
Positional agreement $< 1.0''$							
3.6	63	7.9	70.6	3.0	-7.6	8.5	-0.9
4.5	56	7.5	61.9	2.8	-5.9	8.0	-0.7
5.8	47	6.9	46.9	2.4	0.1	7.3	0.0
8.0	28	5.3	25.1	1.8	2.9	5.6	0.5
Positional agreement $< 2.0''$							
3.6	260	16.1	266.5	5.8	-6.5	17.1	-0.4
4.5	215	14.7	236.9	5.4	-21.9	15.6	-1.4
5.8	173	13.2	173.0	4.7	0.0	14.0	0.0
8.0	100	10.0	97.6	3.5	2.4	10.6	0.2

Table 7. IR and X-Ray Sources Coinciding within 1'' (No Physical Association Implied)

IR Sources (Ramírez et al. 2008)							X-Ray Sources (Muno et al. 2003)				
Name	R.A. (deg)	Dec. (deg)	[3.6]	[4.5]	[5.8]	[8.0]	Name	R.A. (deg)	Dec. (deg)	Spectrum ^a	Δ (") ^b
SSTGC 0469964	266.33191	-29.02930	11.54	11.59	CXOGCJ174519.7-290146	266.33212	-29.02947	soft	0.91
SSTGC 0470990	266.33348	-29.04629	11.15	CXOGCJ174520.0-290246	266.33374	-29.04620	hard	0.87
SSTGC 0473500	266.33735	-29.03927	8.91	8.17	CXOGCJ174521.0-290221	266.33755	-29.03930	hard	0.64
SSTGC 0476142	266.34154	-28.99323	9.85	9.68	CXOGCJ174521.9-285936	266.34134	-28.99344	hard	0.99
SSTGC 0476234	266.34169	-29.00903	9.42	8.95	8.30	...	CXOGCJ174521.9-290032	266.34159	-29.00908	soft	0.36
SSTGC 0477415	266.34345	-29.01875	9.28	9.21	8.77	8.55	CXOGCJ174522.4-290107	266.34369	-29.01881	hard	0.79
SSTGC 0479734	266.34707	-28.95763	9.43	9.33	8.90	...	CXOGCJ174523.2-285727	266.34682	-28.95750	soft	0.92
SSTGC 0479445	266.34664	-29.01752	10.12	9.34	9.28	9.41	CXOGCJ174523.2-290103	266.34684	-29.01764	hard	0.77
SSTGC 0481996	266.35058	-28.97954	9.93	9.51	9.21	9.32	CXOGCJ174524.1-285845	266.35064	-28.97932	soft	0.82
SSTGC 0482409	266.35126	-29.03542	10.02	9.90	9.44	...	CXOGCJ174524.3-290208	266.35145	-29.03561	soft	0.91
SSTGC 0483850	266.35344	-29.00869	10.44	CXOGCJ174524.7-290031	266.35326	-29.00888	hard	0.89
SSTGC 0484205	266.35400	-29.04215	9.62	9.57	9.28	...	CXOGCJ174525.0-290232	266.35419	-29.04226	hard	0.71
SSTGC 0485202	266.35557	-29.02035	11.64	11.09	CXOGCJ174525.2-290113	266.35539	-29.02049	hard	0.75
SSTGC 0487698	266.35948	-28.99733	8.92	8.10	7.59	7.51	CXOGCJ174526.3-285949	266.35961	-28.99721	hard	0.60
SSTGC 0492659	266.36710	-28.99540	9.23	CXOGCJ174528.0-285943	266.36702	-28.99547	hard	0.36
SSTGC 0492380	266.36669	-29.00646	10.18	9.96	CXOGCJ174528.0-290023	266.36680	-29.00644	soft	0.36
SSTGC 0493525	266.36850	-29.05255	11.22	10.93	CXOGCJ174528.4-290308	266.36841	-29.05230	hard	0.93
SSTGC 0494379	266.36984	-28.99134	10.28	...	9.88	...	CXOGCJ174528.7-285928	266.36960	-28.99120	hard	0.91
SSTGC 0494207	266.36958	-29.01202	9.74	9.65	9.07	8.93	CXOGCJ174528.7-290042	266.36979	-29.01183	hard	0.96
SSTGC 0494633	266.37021	-28.95736	10.68	10.21	10.10	...	CXOGCJ174528.8-285726	266.37030	-28.95749	soft	0.55
SSTGC 0495190	266.37111	-29.06847	6.41	5.81	5.19	5.36	CXOGCJ174529.0-290406	266.37109	-29.06846	hard	0.08
SSTGC 0496104	266.37251	-29.00714	11.67	11.38	CXOGCJ174529.4-290025	266.37254	-29.00699	hard	0.56
SSTGC 0496570	266.37324	-29.03733	9.47	9.42	CXOGCJ174529.5-290215	266.37326	-29.03754	soft	0.75
SSTGC 0496855	266.37365	-28.95047	11.79	CXOGCJ174529.6-285701	266.37370	-28.95046	hard	0.16
SSTGC 0496842	266.37363	-28.97793	10.30	9.69	9.50	...	CXOGCJ174529.6-285840	266.37370	-28.97790	hard	0.25
SSTGC 0496808	266.37358	-29.00602	10.78	10.42	CXOGCJ174529.6-290021	266.37375	-29.00607	hard	0.57
SSTGC 0496815	266.37359	-29.04089	9.32	9.20	CXOGCJ174529.6-290227	266.37363	-29.04084	hard	0.23
SSTGC 0498139	266.37558	-29.04694	9.15	8.53	8.12	8.32	CXOGCJ174530.0-290248	266.37530	-29.04681	hard	1.00
SSTGC 0498461	266.37611	-29.06168	10.29	10.24	10.02	...	CXOGCJ174530.3-290341	266.37628	-29.06157	hard	0.67
SSTGC 0500061	266.37851	-29.02794	7.03	5.84	5.04	4.79	CXOGCJ174530.8-290139	266.37864	-29.02777	hard	0.73
SSTGC 0502935	266.38299	-29.04974	7.01	6.92	6.51	6.44	CXOGCJ174531.9-290258	266.38306	-29.04952	hard	0.83
SSTGC 0503729	266.38422	-29.02490	...	9.80	CXOGCJ174532.1-290130	266.38416	-29.02509	hard	0.72
SSTGC 0503925	266.38452	-29.05826	...	10.48	CXOGCJ174532.2-290329	266.38439	-29.05829	hard	0.43
SSTGC 0504458	266.38536	-28.98557	9.86	9.96	9.64	...	CXOGCJ174532.5-285908	266.38566	-28.98556	hard	0.94

Table 7—Continued

IR Sources (Ramírez at al. 2008)							X-Ray Sources (Muno et al. 2003)				
Name	R.A. (deg)	Dec. (deg)	[3.6]	[4.5]	[5.8]	[8.0]	Name	R.A. (deg)	Dec. (deg)	Spectrum ^a	Δ (") ^b
SSTGC 0505766	266.38734	-29.07664	10.91	10.56	CXOGCJ174532.8-290436	266.38703	-29.07670	hard	1.00
SSTGC 0507145	266.38945	-28.94431	10.81	10.43	9.89	...	CXOGCJ174533.4-285638	266.38941	-28.94415	soft	0.58
SSTGC 0508028	266.39072	-28.95800	11.45	10.97	CXOGCJ174533.7-285728	266.39077	-28.95803	soft	0.19
SSTGC 0507814	266.39043	-29.07579	9.62	8.73	8.37	...	CXOGCJ174533.7-290432	266.39053	-29.07578	hard	0.32
SSTGC 0508562	266.39155	-28.99906	9.42	CXOGCJ174534.0-285956	266.39182	-28.99901	hard	0.87
SSTGC 0510334	266.39416	-29.04338	7.98	7.73	7.17	6.47	CXOGCJ174534.5-290236	266.39409	-29.04357	hard	0.73
SSTGC 0510970	266.39515	-29.07890	7.48	7.39	6.80	6.98	CXOGCJ174534.8-290444	266.39535	-29.07906	hard	0.84
SSTGC 0511940	266.39659	-28.97869	8.27	...	CXOGCJ174535.1-285843	266.39633	-28.97877	hard	0.87
SSTGC 0511999	266.39668	-29.01359	8.57	8.45	7.86	7.22	CXOGCJ174535.2-290048	266.39689	-29.01352	hard	0.71
SSTGC 0512567	266.39755	-28.93489	9.50	9.57	9.27	...	CXOGCJ174535.4-285605	266.39763	-28.93492	hard	0.28
SSTGC 0514496	266.40052	-28.94409	8.82	8.26	7.97	7.82	CXOGCJ174536.1-285638	266.40059	-28.94407	soft	0.23
SSTGC 0514528	266.40057	-28.96362	10.20	10.36	9.89	...	CXOGCJ174536.1-285748	266.40067	-28.96347	hard	0.62
SSTGC 0514886	266.40111	-28.97721	8.17	CXOGCJ174536.3-285837	266.40125	-28.97712	hard	0.55
SSTGC 0515077	266.40139	-29.02929	10.73	10.41	CXOGCJ174536.3-290145	266.40150	-29.02919	soft	0.51
SSTGC 0515409	266.40189	-29.02083	9.30	CXOGCJ174536.4-290114	266.40181	-29.02067	hard	0.64
SSTGC 0517465	266.40502	-28.98550	8.15	8.16	7.79	...	CXOGCJ174537.2-285906	266.40502	-28.98526	hard	0.87
SSTGC 0518345	266.40641	-29.03129	10.04	9.92	9.80	...	CXOGCJ174537.5-290153	266.40653	-29.03142	hard	0.62
SSTGC 0518659	266.40684	-29.00667	9.45	CXOGCJ174537.6-290023	266.40683	-29.00657	hard	0.36
SSTGC 0519255	266.40776	-29.02434	9.93	9.76	8.65	7.41	CXOGCJ174537.8-290127	266.40757	-29.02426	soft	0.66
SSTGC 0519545	266.40824	-29.02626	8.25	8.13	CXOGCJ174537.9-290134	266.40831	-29.02622	soft	0.26
SSTGC 0520087	266.40907	-28.98803	8.26	...	CXOGCJ174538.1-285916	266.40878	-28.98805	hard	0.92
SSTGC 0520903	266.41025	-28.96968	8.50	8.45	7.91	7.69	CXOGCJ174538.4-285810	266.41031	-28.96958	hard	0.40
SSTGC 0521476	266.41115	-29.01893	...	8.51	CXOGCJ174538.6-290107	266.41101	-29.01889	hard	0.47
SSTGC 0522739	266.41312	-28.96061	9.19	9.22	8.79	8.46	CXOGCJ174539.1-285738	266.41308	-28.96081	hard	0.73
SSTGC 0522856	266.41327	-29.04730	11.06	8.88	8.23	8.20	CXOGCJ174539.2-290250	266.41356	-29.04738	hard	0.95
SSTGC 0523283	266.41392	-29.00467	8.12	CXOGCJ174539.3-290016	266.41397	-29.00467	soft	0.16
SSTGC 0523729	266.41463	-29.02514	9.49	8.94	8.81	...	CXOGCJ174539.5-290129	266.41465	-29.02499	hard	0.54
SSTGC 0524504	266.41584	-29.00847	5.63	CXOGCJ174539.7-290029	266.41567	-29.00827	soft	0.91
SSTGC 0525460	266.41726	-28.99969	6.18	4.59	3.16	1.69	CXOGCJ174540.1-285957	266.41718	-28.99944	hard	0.92
SSTGC 0525510	266.41735	-29.01540	8.21	...	6.98	...	CXOGCJ174540.1-290055	266.41733	-29.01546	soft	0.23
SSTGC 0525714	266.41765	-28.98358	8.52	8.46	7.72	6.99	CXOGCJ174540.2-285900	266.41753	-28.98360	hard	0.38
SSTGC 0526867	266.41944	-28.94462	8.58	CXOGCJ174540.6-285640	266.41950	-28.94445	soft	0.65
SSTGC 0527316	266.42016	-29.03007	8.12	...	CXOGCJ174540.8-290149	266.42011	-29.03029	hard	0.80
SSTGC 0527347	266.42020	-29.05794	11.12	CXOGCJ174540.8-290328	266.42037	-29.05804	soft	0.65

Table 7—Continued

IR Sources (Ramírez at al. 2008)							X-Ray Sources (Muno et al. 2003)				
Name	R.A. (deg)	Dec. (deg)	[3.6]	[4.5]	[5.8]	[8.0]	Name	R.A. (deg)	Dec. (deg)	Spectrum ^a	Δ (") ^b
SSTGC 0527844	266.42100	-29.00472	8.56	7.16	CXOGCJ174541.0-290017	266.42095	-29.00489	hard	0.62
SSTGC 0529789	266.42400	-29.00790	9.01	CXOGCJ174541.7-290027	266.42377	-29.00774	hard	0.93
SSTGC 0530322	266.42482	-28.99881	8.47	...	CXOGCJ174541.9-285955	266.42473	-28.99865	hard	0.65
SSTGC 0531615	266.42680	-28.96723	9.28	CXOGCJ174542.4-285802	266.42678	-28.96724	hard	0.07
SSTGC 0532179	266.42763	-28.95284	11.30	10.80	CXOGCJ174542.6-285709	266.42768	-28.95257	hard	0.99
SSTGC 0532570	266.42818	-28.97533	9.54	9.29	8.87	...	CXOGCJ174542.7-285831	266.42816	-28.97552	hard	0.68
SSTGC 0533119	266.42903	-29.07535	...	10.74	CXOGCJ174542.9-290431	266.42890	-29.07535	soft	0.41
SSTGC 0533640	266.42983	-29.01391	7.39	6.73	6.11	5.85	CXOGCJ174543.1-290049	266.42961	-29.01382	soft	0.76
SSTGC 0533886	266.43016	-28.98839	10.20	10.18	9.59	...	CXOGCJ174543.2-285917	266.43035	-28.98822	hard	0.85
SSTGC 0534588	266.43123	-28.98360	9.10	...	9.08	...	CXOGCJ174543.4-285900	266.43102	-28.98341	hard	0.96
SSTGC 0534566	266.43120	-29.06347	8.47	8.36	7.85	7.97	CXOGCJ174543.4-290347	266.43106	-29.06327	hard	0.83
SSTGC 0535312	266.43230	-29.02660	11.89	10.66	CXOGCJ174543.7-290136	266.43234	-29.02668	hard	0.32
SSTGC 0535628	266.43280	-29.04581	9.84	9.81	9.31	...	CXOGCJ174543.9-290245	266.43309	-29.04590	hard	0.96
SSTGC 0535765	266.43300	-29.08237	9.46	9.48	9.43	9.48	CXOGCJ174543.9-290456	266.43305	-29.08238	soft	0.16
SSTGC 0536043	266.43341	-29.07468	10.24	9.67	9.44	9.04	CXOGCJ174544.0-290428	266.43363	-29.07460	hard	0.75
SSTGC 0537314	266.43533	-28.97495	9.36	8.80	8.24	7.83	CXOGCJ174544.4-285829	266.43531	-28.97486	hard	0.32
SSTGC 0537395	266.43544	-28.97053	6.76	...	CXOGCJ174544.5-285813	266.43557	-28.97044	hard	0.52
SSTGC 0537801	266.43609	-29.06095	12.55	CXOGCJ174544.7-290339	266.43631	-29.06109	hard	0.87
SSTGC 0539467	266.43859	-28.97468	10.76	10.45	CXOGCJ174545.2-285828	266.43870	-28.97466	soft	0.36
SSTGC 0539388	266.43847	-29.04029	12.23	12.24	CXOGCJ174545.2-290224	266.43840	-29.04009	soft	0.75
SSTGC 0543526	266.44459	-29.05783	10.56	CXOGCJ174546.6-290328	266.44449	-29.05786	soft	0.33
SSTGC 0543690	266.44482	-29.03528	8.35	CXOGCJ174546.7-290207	266.44473	-29.03552	hard	0.92
SSTGC 0544019	266.44530	-29.04789	9.47	8.58	7.83	...	CXOGCJ174546.8-290252	266.44521	-29.04789	soft	0.28
SSTGC 0546444	266.44903	-28.94019	7.82	7.48	6.85	6.78	CXOGCJ174547.7-285624	266.44899	-28.94008	hard	0.41
SSTGC 0547195	266.45015	-29.05055	7.54	7.26	6.80	6.89	CXOGCJ174548.0-290301	266.45010	-29.05040	hard	0.55
SSTGC 0548119	266.45158	-28.99872	9.94	...	CXOGCJ174548.4-285954	266.45179	-28.99852	hard	0.97
SSTGC 0548472	266.45212	-28.96311	10.88	10.62	CXOGCJ174548.5-285747	266.45240	-28.96309	hard	0.88
SSTGC 0548665	266.45244	-29.04621	11.93	CXOGCJ174548.5-290246	266.45248	-29.04616	soft	0.23
SSTGC 0550312	266.45497	-29.02723	10.71	10.72	10.67	...	CXOGCJ174549.1-290137	266.45492	-29.02721	soft	0.18
SSTGC 0550210	266.45481	-29.08411	10.33	9.94	9.58	9.10	CXOGCJ174549.1-290502	266.45467	-29.08396	soft	0.71
SSTGC 0550863	266.45578	-28.95373	8.27	8.02	7.54	7.52	CXOGCJ174549.4-285712	266.45597	-28.95356	hard	0.87
SSTGC 0553475	266.45968	-29.00568	12.25	11.87	CXOGCJ174550.2-290020	266.45948	-29.00566	hard	0.63
SSTGC 0554271	266.46090	-28.98878	9.63	9.00	8.63	7.90	CXOGCJ174550.6-285919	266.46096	-28.98886	soft	0.36
SSTGC 0554555	266.46134	-29.07635	12.52	11.67	CXOGCJ174550.7-290434	266.46159	-29.07628	soft	0.83

Table 7—Continued

IR Sources (Ramírez et al. 2008)							X-Ray Sources (Muno et al. 2003)				Δ (") ^b
Name	R.A. (deg)	Dec. (deg)	[3.6]	[4.5]	[5.8]	[8.0]	Name	R.A. (deg)	Dec. (deg)	Spectrum ^a	
SSTGC 0558398	266.46721	-28.96776	9.82	9.85	9.51	...	CXOGCJ174552.1-285804	266.46722	-28.96790	soft	0.50
SSTGC 0559457	266.46887	-28.99130	7.42	...	CXOGCJ174552.5-285928	266.46878	-28.99131	hard	0.29
SSTGC 0560119	266.46985	-29.03013	10.41	CXOGCJ174552.7-290148	266.46965	-29.03021	hard	0.69
SSTGC 0564995	266.47723	-29.04817	11.86	11.62	CXOGCJ174554.5-290252	266.47709	-29.04805	soft	0.62
SSTGC 0570573	266.48573	-28.96011	10.59	10.53	11.08	...	CXOGCJ174556.5-285736	266.48560	-28.96019	soft	0.50
SSTGC 0572280	266.48837	-29.05031	9.12	9.07	8.67	...	CXOGCJ174557.2-290301	266.48852	-29.05042	hard	0.61
SSTGC 0572559	266.48879	-28.96801	9.52	9.09	CXOGCJ174557.3-285804	266.48899	-28.96787	hard	0.80
SSTGC 0575612	266.49335	-29.02236	8.91	8.90	8.62	8.92	CXOGCJ174558.4-290120	266.49364	-29.02232	soft	0.93
SSTGC 0577500	266.49625	-29.04868	10.02	9.83	9.44	10.04	CXOGCJ174559.1-290255	266.49640	-29.04875	hard	0.53
SSTGC 0578722	266.49813	-29.00052	10.09	9.93	9.74	...	CXOGCJ174559.5-290002	266.49806	-29.00067	soft	0.59
SSTGC 0579221	266.49888	-28.98583	9.61	9.60	9.26	9.22	CXOGCJ174559.7-285908	266.49881	-28.98571	hard	0.47
SSTGC 0580810	266.50121	-29.01808	...	11.52	CXOGCJ174600.2-290105	266.50108	-29.01809	soft	0.41
SSTGC 0588034	266.51210	-29.01352	...	10.80	CXOGCJ174602.8-290049	266.51202	-29.01366	hard	0.56

Note. — Positional coincidence does not necessarily imply a physical association of IR and X-ray sources. In fact, $\sim 70\%$ of the objects on this list are likely to be random positional coincidences of unrelated sources along the line of sight.

^asoft = detected in the 0.5–2.0 keV band; hard = not detected in the 0.5–2.0 keV band.

^bSeparation between IR and X-ray source positions.

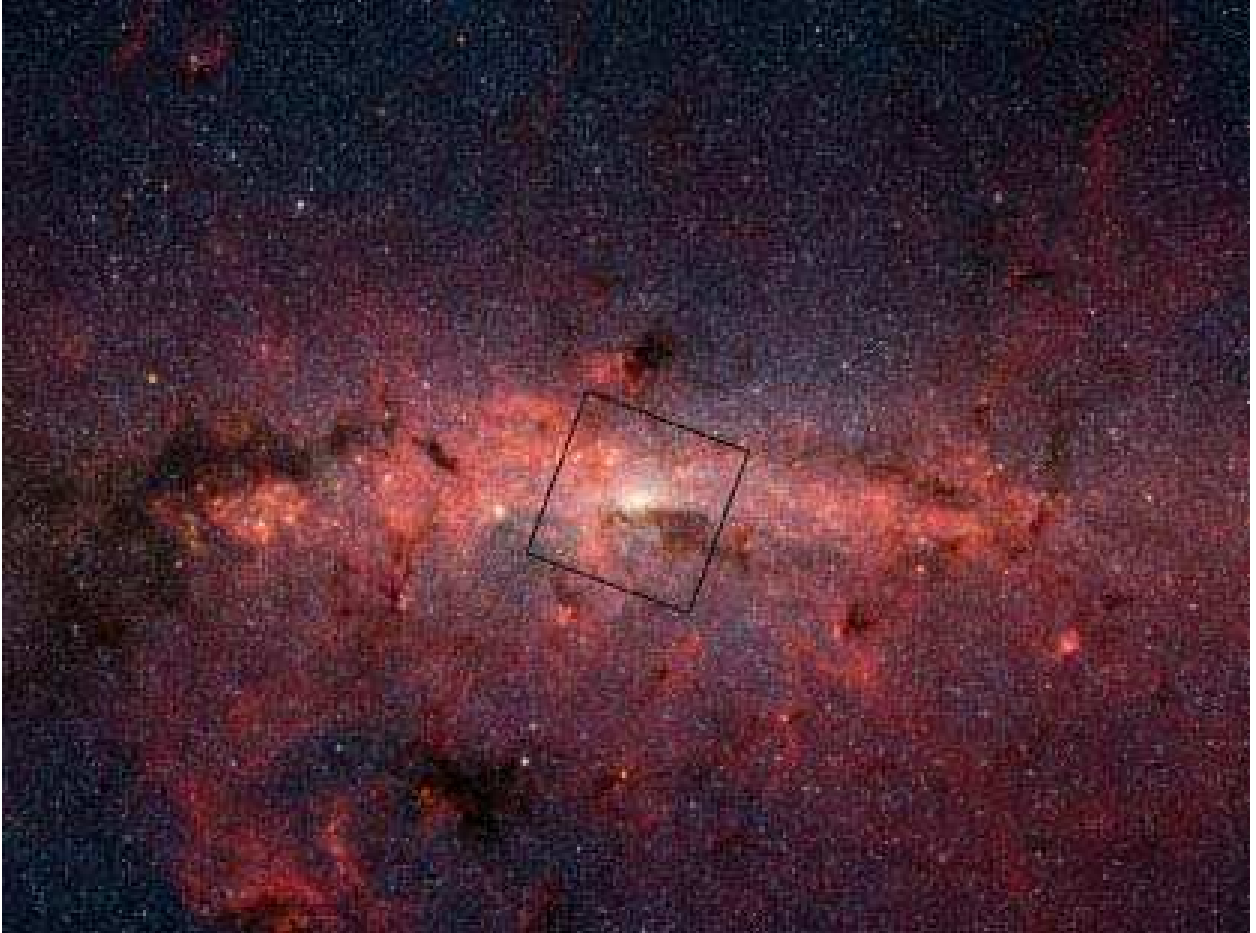


Fig. 1.— Our *Spitzer*/IRAC Galactic Center Survey mosaic image (Stolovy et al. 2006), showing the 40×40 pc X-ray comparison field (square outline). This image is centered at $(l, b) = (0.0, 0.0)$ and is displayed in galactic coordinates.



Fig. 2.— The 40×40 parsec infrared and X-ray field that was used for the X-ray/infrared point source correlation study. *Left:* Composite 3.6 (blue), 5.8 (green) and $8.0 \mu\text{m}$ (red) *Spitzer*/IRAC image of the 40×40 parsec study field. It yielded $\sim 20,000$ infrared point sources. *Right:* Composite Chandra image of the study field (Wang et al. 2002); red = 1 - 3 keV, green = 3 - 5 keV, blue = 5 - 8 keV. Equatorial north is up, east is right.

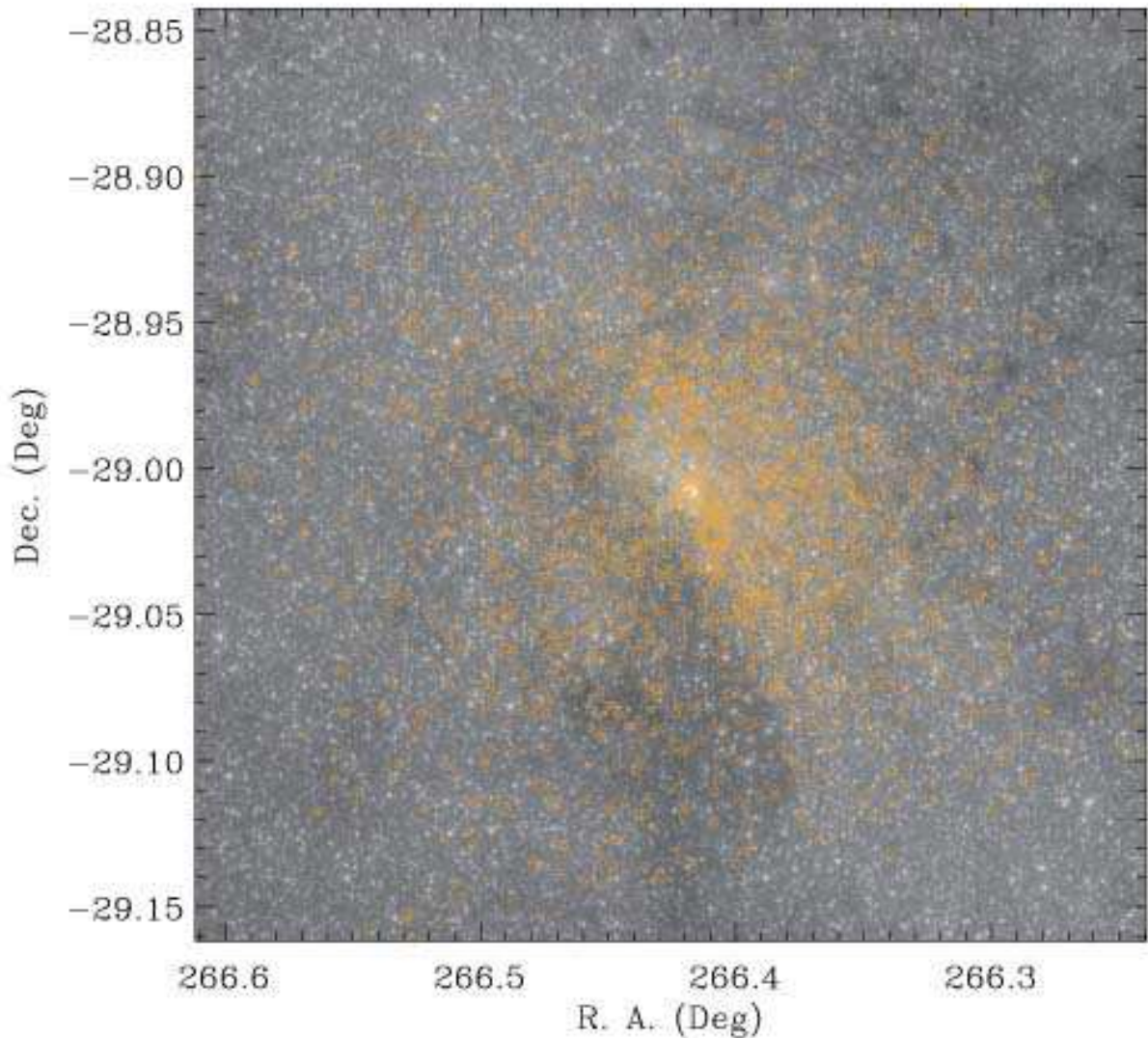


Fig. 3.— (a) Our *Spitzer*/IRAC 3.6 μm image, showing the $\sim 20,000$ compact infrared sources brighter than $[3.6] = 12$ that we extracted in a 40×40 parsec subset of the survey region (Ramírez et al. 2008), overlaid with 2357 hard and soft X-ray sources (orange circles) identified by Munro et al. (2003). (b) The same 3.6 μm image is shown. Here, only the X-ray point sources that fell within $0''.5$ (blue), $1''$ (green), and $2''$ (red) of a 3.6 μm source are indicated. Hard X-ray sources are indicated by crosses; soft sources are indicated by circles. The six white squares indicate the locations of the massive young stars studied by Munro et al. (2006). All six are detected by IRAC, but only three are X-ray sources.

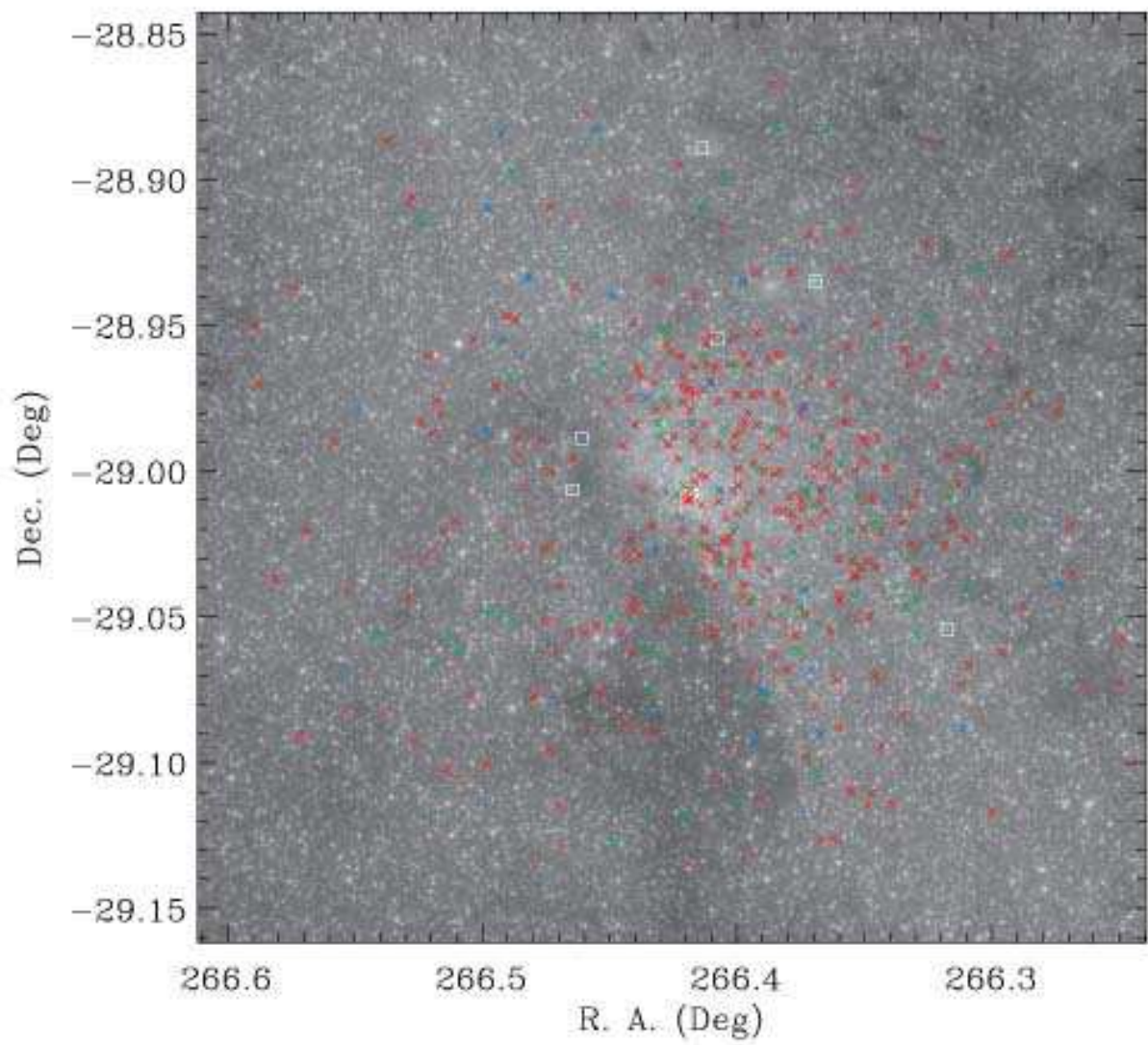


Fig. 3. — Continued.

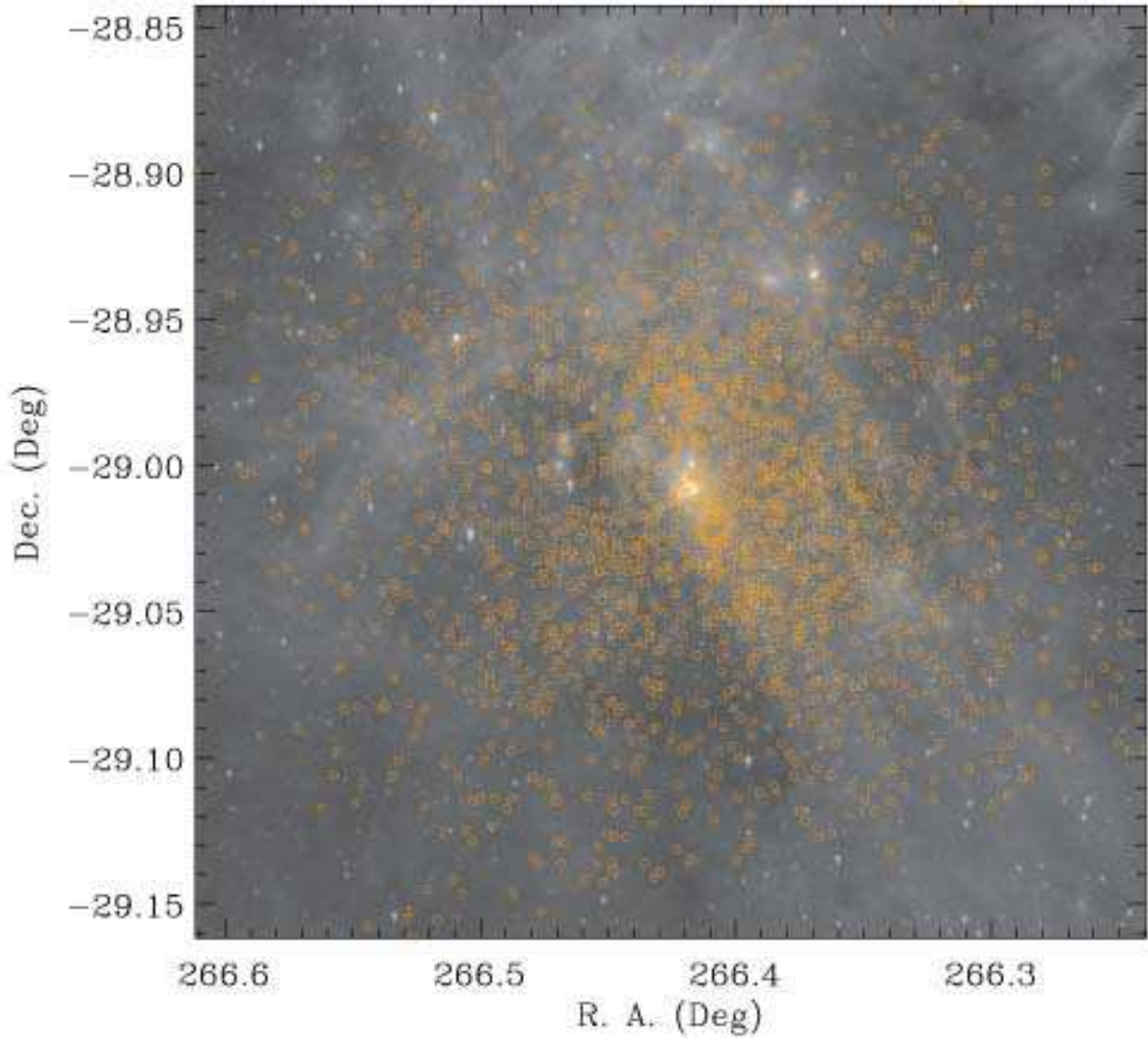


Fig. 4.— (a) Our *Spitzer*/IRAC 8.0 μm image, overlaid with the 2178 X-ray sources without IR counterparts (orange circles). (b) The same 8.0 μm image is shown. Here, only the X-ray point sources that fell within $0''.5$ (blue), $1''$ (green), and $2''$ (red) of an 8.0 μm source are indicated. Hard X-ray sources are indicated by crosses; soft sources are indicated by circles. The six white squares indicate the locations of the massive young stars studied by Munoz et al. (2006). All six are detected by IRAC, but only three are X-ray sources.

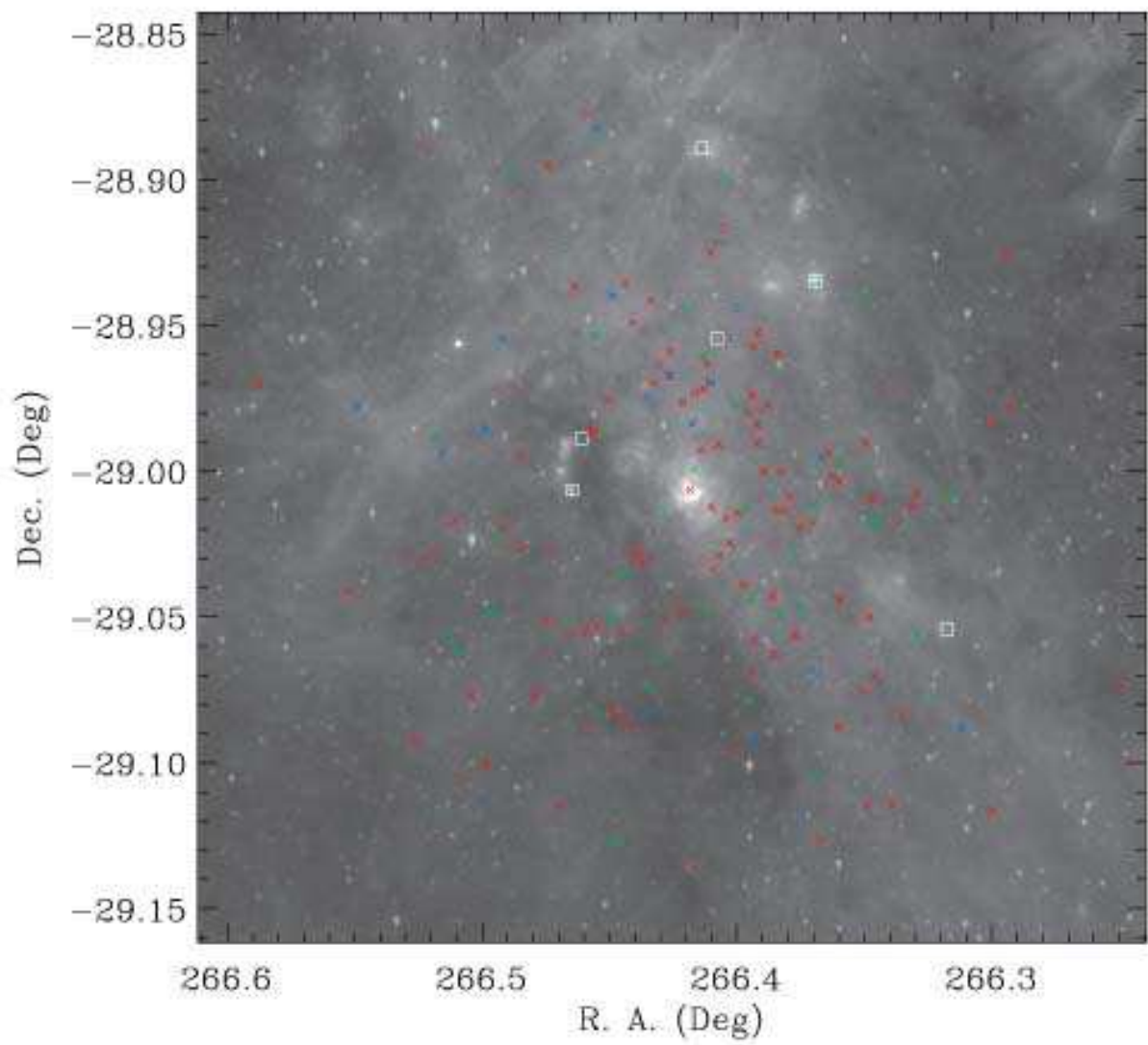


Fig. 4. — Continued.

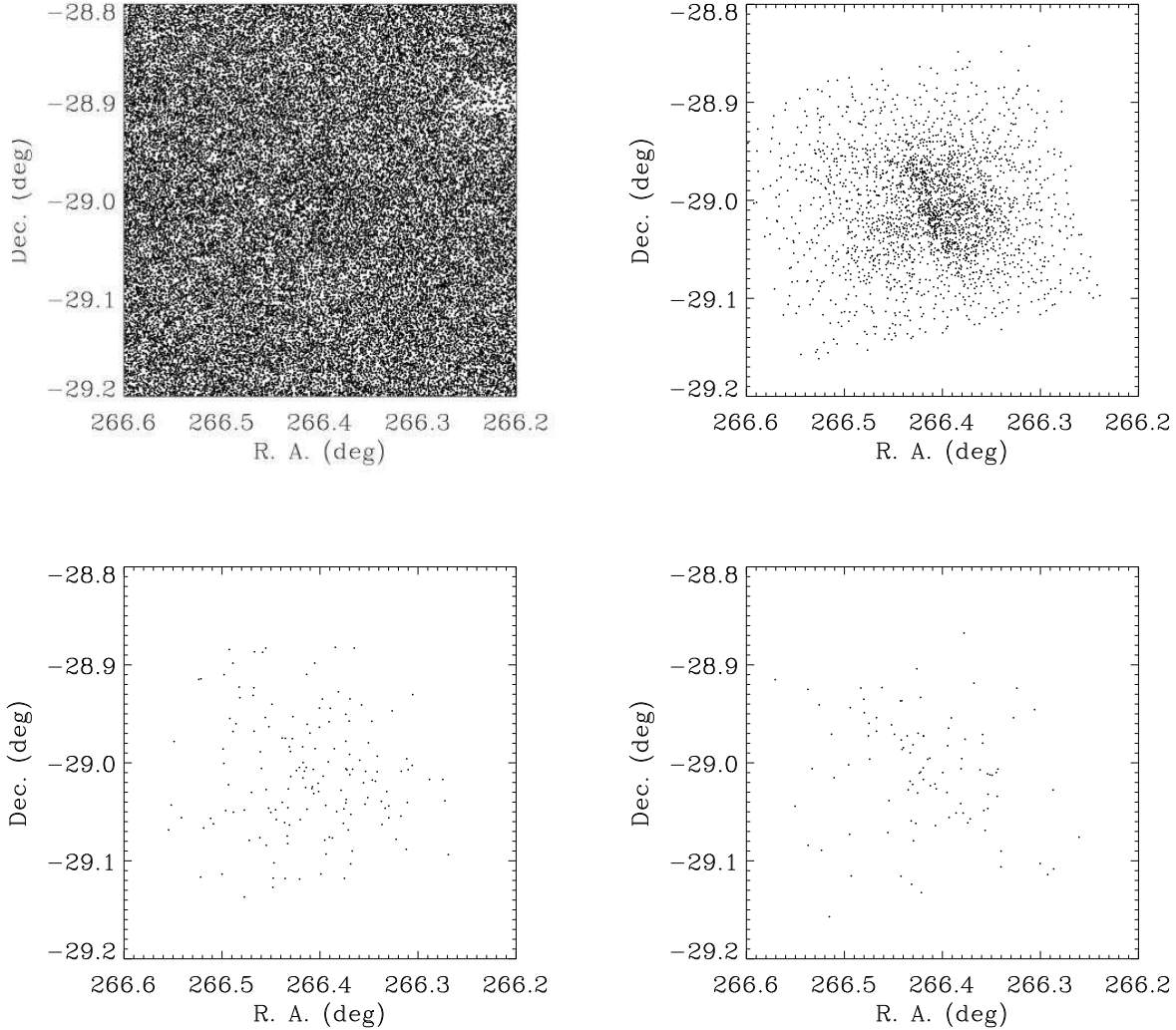


Fig. 5.— (a) Positions of all $\sim 20,000$ $3.6 \mu\text{m}$ sources (black dots) in the 40×40 pc study field from our *Spitzer*/IRAC Galactic Center survey. (b) Positions of all 2357 X-ray sources in the Muno et al. (2003) survey. (c) Positions of the 156 IRAC $3.6 \mu\text{m}$ sources that fall within $1''$ of an X-ray source in the Muno et al. (2003) sample, a correlation of about 7%. (d) Shifting the position template by $5''$ from the source positions in (a) results in an average of 120 IRAC $3.6 \mu\text{m}$ sources within $1''$ of X-ray source, suggesting that these are chance associations. The actual correlation of $3.6 \mu\text{m}$ and X-ray point sources within $1''$ is therefore probably not greater than 2%.

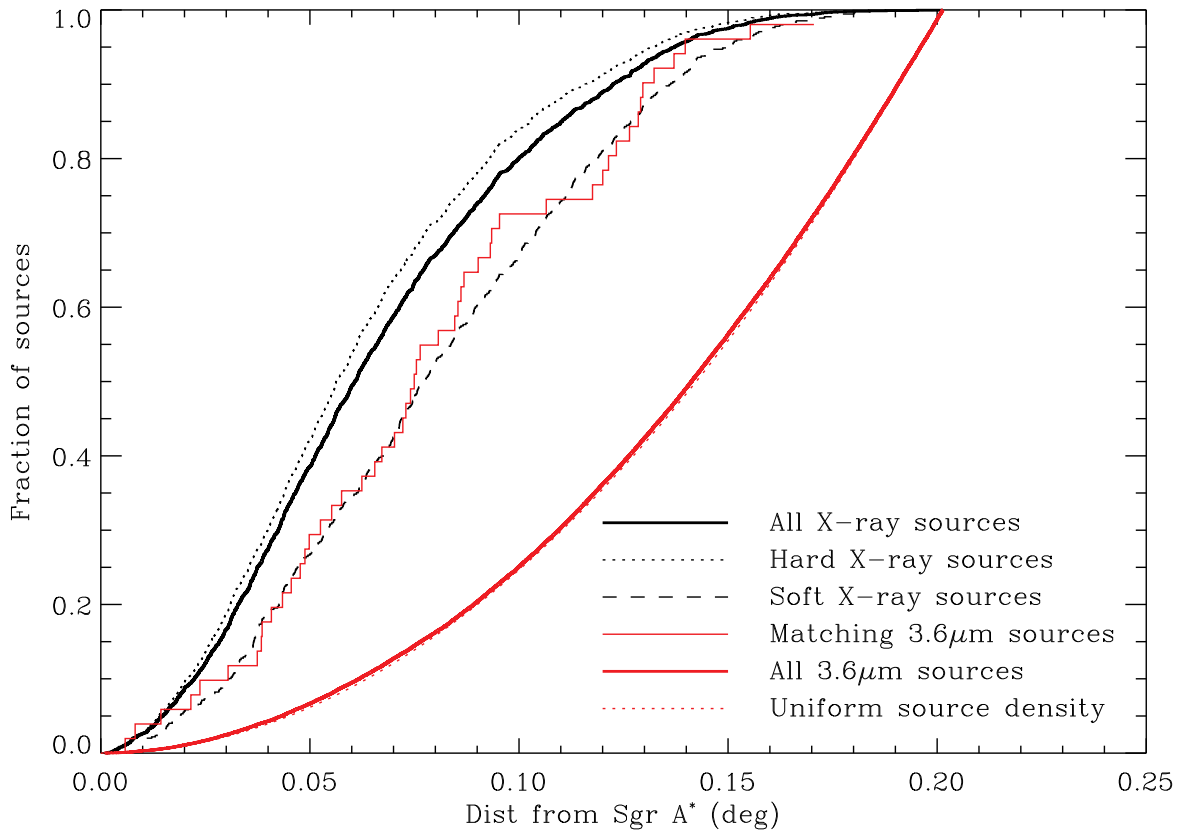


Fig. 6.— The cumulative radial distributions with respect to Sgr A* are shown from all X-ray sources, only the hard sources, only the soft sources, and only the sources with matching $3.6 \mu\text{m}$ sources within $0''.5$. The K-S test indicates that the hard sources have a statically different distribution than the soft sources and the sources with IR counterparts. The distributions of soft sources and sources with $3.6 \mu\text{m}$ counterparts are *not* significantly different. The thick red line shows the corresponding distribution for all $3.6 \mu\text{m}$ sources within the same region as the X-ray sources. This distribution differs only slightly from that expected for a uniform source density across the region.

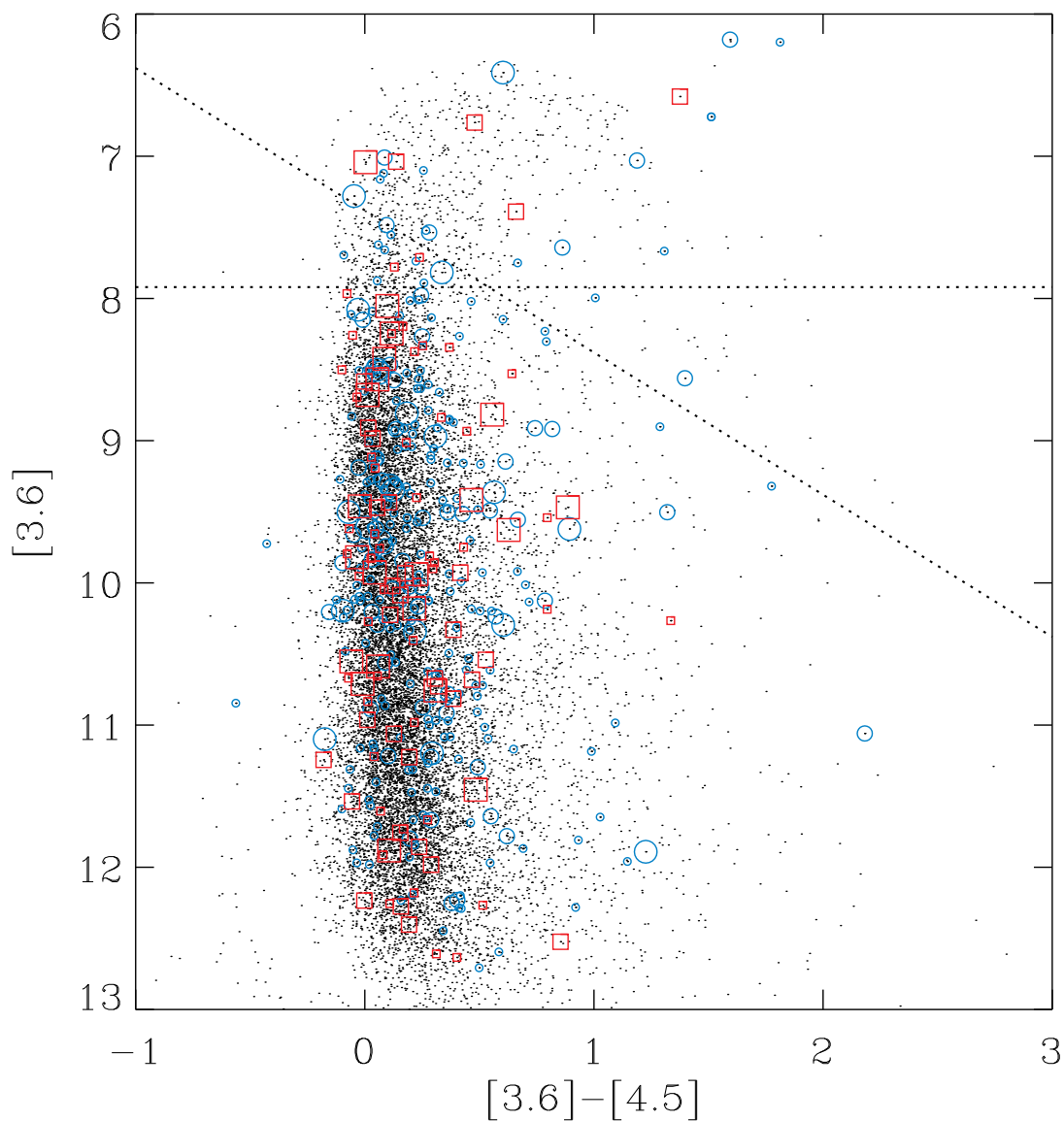


Fig. 7.— IR stars with X-ray candidates have typical colors. Color-magnitude diagram for 17613 IRAC sources (small black dots) that were detected in both channels 1 and 2 ($3.6 \mu\text{m}$ and $4.5 \mu\text{m}$) in the 40×40 parsec study region. 42 X-ray sources had IRAC sources lying within $0''.5$ of the nominal X-ray positions (large symbols), 130 had IRAC sources within $1''$ (medium symbols), and 394 had IRAC sources within $2''$ (small symbols). Square symbols indicate soft X-ray sources; circles indicate hard X-ray sources. The horizontal and diagonal dotted lines indicate the levels at which saturation may begin to affect the 3.6 and $4.5 \mu\text{m}$ photometry respectively (Ramírez et al. 2008).

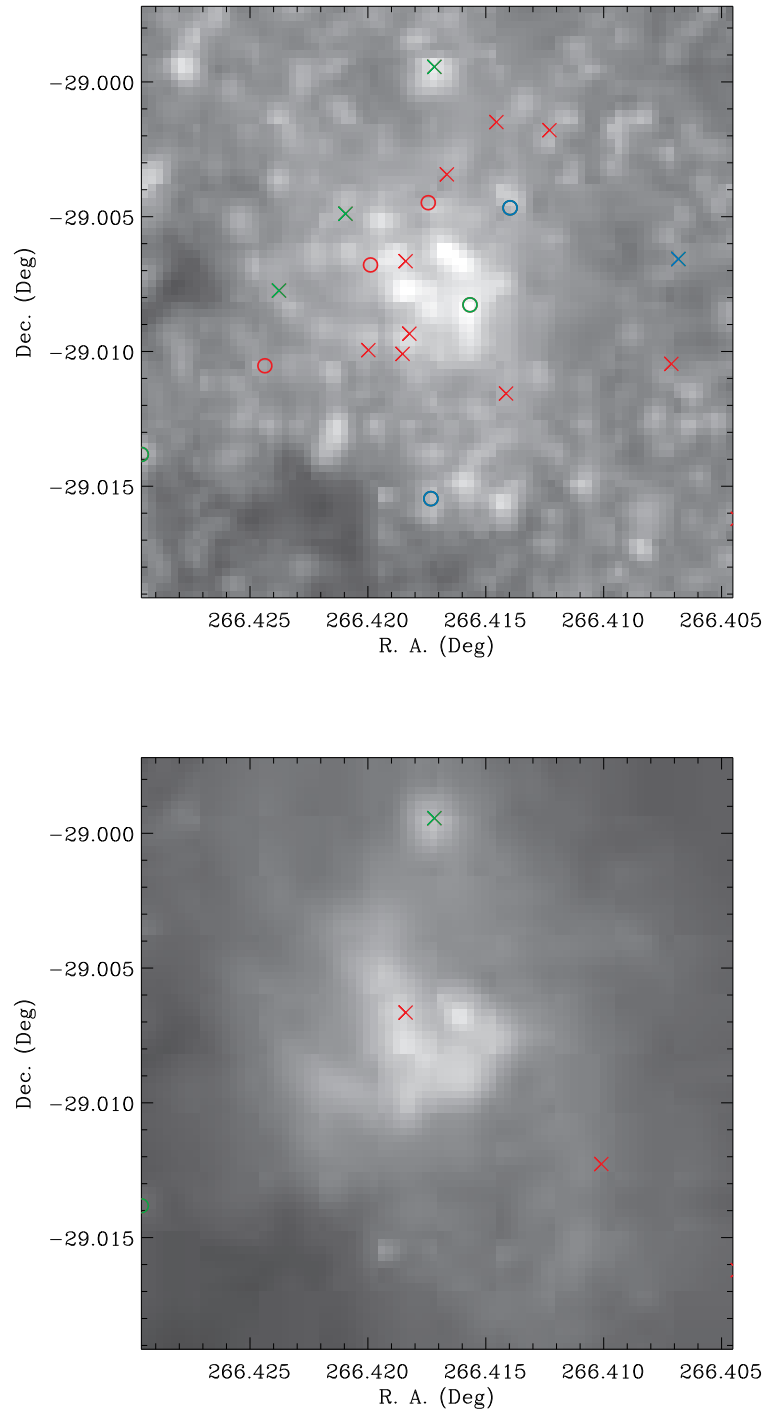


Fig. 8.— (top) An enlarged view of matching X-ray and 3.6 μm point sources at the Galactic Center cluster. Matching sources within 0".5, 1" and 2" are indicated by blue, green and red symbols, respectively. Hard X-ray sources are indicated by crosses; soft sources are indicated by circles. IRS 13 is at the green circle nearest to the center of the image. (bottom) The same view at 8 μm with the matching X-ray and 8 μm point sources superimposed.